Construction and validation of a predictive model of pathological complete response combined with MRI and tumor indicators for HER2-positive breast cancer after neoadjuvant targeted therapy

KEYING ZHU[1,2*], ZEYING LI[1*], JIAQIAN LIAO[1*], CHANGAN WANG[1], RONG GUO[1], YIYIN TANG[1], SHAOQIANG ZHOU[1], YINGYING DING[3], DEDIAN CHEN[1], JIANKUI WANG[1], JIANYUN NIE[1] and SHENG HUANG[1]

[1]Yunnan Key Laboratory of Breast Cancer Precision Medicine, Department of Breast Surgery, Breast Cancer Center of The Third Affiliated Hospital of Kunming Medical University, Yunnan Cancer Hospital, Yunnan Cancer Centre, Peking University Cancer Hospital Yunnan Hospital, Kunming, Yunnan 650118, P.R. China; [2]Comprehensive Surgery Department of Qujing Maternal and Child Health-Care Hospital, Affiliated Maternal and Child Health-Care Hospital of Kunming University of Science and Technology, Qujing, Yunnan 655000, P.R. China; [3]Department of Radiology, The Third Affiliated Hospital of Kunming Medical University, Yunnan Cancer Hospital, Yunnan Cancer Centre, Peking University Cancer Hospital Yunnan, Kunming, Yunnan 650118, P.R. China

Received November 5, 2025; Accepted April 22, 2026

DOI: 10.3892/ol.2026.15693

Abstract. Accurate models for predicting pathological complete response (pCR) after neoadjuvant therapy (NAT) are increasingly needed in patients with human epidermal growth factor receptor 2 (HER2)-positive breast cancer (BC). In the present study, a nomogram was developed to estimate the probability of achieving a pCR in this population. Clinical data were retrospectively and prospectively collected from patients with HER2-positive BC at three time points: Before NAT, after the first cycle of neoadjuvant targeted therapy and after the completion of NAT before surgery. Logistic regression analysis was performed to identify independent predictors of pCR, and these variables were used to construct a predictive model and corresponding nomogram. Model performance was evaluated using calibration curves, decision curve analysis, receiver operating characteristic (ROC) curves and the area under the ROC curve (AUC), with retrospective data and prospective data used for internal and external validations, respectively. Logistic regression analysis of the retrospective cohort identified eight predictors associated with pCR, which were incorporated into a concise nomogram. Internal validation demonstrated good calibration and strong predictive performance, with an AUC value of 0.886 (P<0.001), sensitivity of 0.822 and specificity of 0.818. External validation further confirmed the excellent discriminatory ability of the model, yielding an AUC value of 0.961 (P<0.001), sensitivity of 1.000 and specificity was 0.875. Overall, this nomogram, which integrates multiple clinically relevant factors, may serve as a useful tool for predicting post-NAT pCR in patients with HER2-positive BC and may support more precise treatment decision-making in clinical practice.

Correspondence to: Professor Sheng Huang or Professor Jianyun Nie, Yunnan Key Laboratory of Breast Cancer Precision Medicine, Department of Breast Surgery, Breast Cancer Center of The Third Affiliated Hospital of Kunming Medical University, Yunnan Cancer Hospital, Yunnan Cancer Centre, Peking University Cancer Hospital Yunnan Hospital, 519 Kunzhou Road, Xishan, Kunming, Yunnan 650118, P.R. China
E-mail: sammer312@126.com
E-mail: njyvip@sina.com

*Contributed equally

Abbreviations: AC, anthracyclines + cyclophosphamide; ADC, apparent diffusion coefficient; AFP, α-fetoprotein; AJCC, American Joint Committee on Cancer; AUC, area under the ROC curve; BC, breast cancer; CA, carbohydrate antigen; CEA, carcinoembryonic antigen; DCA, decision curve analysis; DCE-MRI, dynamic contrast-enhanced magnetic resonance imaging; DWI, diffusion-weighted imaging; ER, estrogen receptor; HER2, human epidermal growth factor receptor 2; HP, Herceptin (trastuzumab) + pertuzumab; NAT, neoadjuvant therapy; NTT, neoadjuvant targeted therapy; pCR, pathological complete response; PR, progesterone receptor; ROC, receiver operating characteristic; SF, serum ferritin; TIC, time intensity curve; VIF, variance inflation factor

Key words: breast cancer, HER2-positive, neoadjuvant therapy response evaluation, nomogram, prediction model

Introduction

Breast cancer (BC) has the second highest age-standardized incidence rate (46.8 per 100,000) among malignant tumors worldwide according to recent global cancer burden data (1). Neoadjuvant therapy (NAT) has become the acknowledged standard treatment for middle- and early-stage BC worldwide (2). NAT offers several clinical advantages, including tumor downstaging, reduction in tumor size to facilitate

breast-conserving surgery, expansion of surgical options, early assessment of treatment response, reduction of systemic tumor burden and improvement of long-term clinical prognosis (3). Pathological complete response (pCR), defined as the absence of residual invasive cancer in the breast and axillary lymph nodes after NAT (4,5), is commonly used as a key endpoint in clinical studies. Achieving a pCR is associated with markedly improved long-term survival outcomes, compared with those have residual tumors (4). Human epidermal growth factor receptor 2 (HER2)-positive BC represents a distinct molecular subtype, characterized by high invasiveness, early metastasis, a poor prognosis and a high risk of recurrence, as well as reduced sensitivity to conventional chemotherapy (5,6). In recent years, the development and clinical application of HER2-targeted therapies and small-molecule inhibitors have substantially improved treatment outcomes (7). In particular, the combination of trastuzumab and pertuzumab with chemotherapy drugs has been shown to be safe and to achieve higher pCR rates (39.38-68%) in multiple studies (8-10).

Magnetic resonance imaging (MRI), particularly the combination of dynamic contrast-enhanced MRI (DCE-MRI) and diffusion weighted imaging (DWI), is currently regarded as a preferred method for evaluating the efficacy of NAT in BC (11). DCE-MRI combined with DWI enables morphological assessment for tumor size and post-treatment contraction patterns in both the primary tumor and axillary lymph nodes, while also providing functional information on water molecule diffusion, cellular metabolism and tumor hemodynamics (12,13). Semi-quantitative parameters, such as the time intensity curve (TIC), and quantitative measures, such as the apparent diffusion coefficient (ADC) value, further reflect the structural and microenvironmental characteristics of tumor tissue (14).

In addition to imaging data, response to NAT can also be reflected by various circulating tumor biomarkers (15). Carcinoembryonic antigen (CEA) is a widely used non-specific tumor marker that is elevated in several malignancies, including colorectal (16), lung (17) and gastric (18) cancer, as well as BC (19). Carbohydrate antigens (CAs), including CA125, CA153, CA19-9, CA724, CA242, represent another group of commonly used markers in clinical practice (19). However, no standardized approach exists regarding the optimal selection or combination of these markers for evaluating NAT response in BC. Therefore, integrating serum tumor markers with imaging data may improve the assessment of treatment response.

Generally, the early prediction and identification of patients likely to achieve a pCR during NAT, using readily available clinical data, can provide valuable guidance for optimizing surgical timing and strategy, as well as subsequent treatment planning (20). Accordingly, the development of predictive models for pathological response in HER2-positive BC following neoadjuvant targeted therapy (NTT) has become an important area of research. In the present study, independent predicators of pCR were identified from pathological features, DCE-MRI imaging parameters and serum tumor biomarkers in patients with HER2-positive BC. Based on these factors, a comprehensive predictive model was developed and presented as a nomogram to facilitate the preoperative estimation of treatment response and support individualized clinical decision-making.

Patients and methods

Study cohorts. The study protocol was reviewed and approved by the institutional ethics committee of the Third Affiliated Hospital of Kunming Medical University, Yunnan Cancer Hospital, Yunnan Cancer Centre, Peking University Cancer Hospital Yunnan Hospital, Kunming, China (approval no. KYLX2022182). Patients were enrolled after a diagnosis of early- or mid-stage (less than stage IV) HER2-positive BC confirmed by preoperative biopsy. Patients were retrospectively included between January 1, 2018, and December 31, 2021, and prospectively enrolled between January 1, 2022, and September 30, 2022, at the Breast Cancer Center of the Third Affiliated Hospital of Kunming Medical University, Yunnan Cancer Hospital (Kunming, China). Inclusion criteria were as follows: i) Newly diagnosed early- or mid-stage (less than stage IV) HER2-positive BC; ii) completion of full-course NAT combining targeted therapy and chemotherapy; iii) surgery performed after NAT with available pathological results; and iv) complete MRI and hematological data at baseline, after the first cycle of NTT, and after completion of NAT prior to surgery. The exclusion criteria were as follows: i) Incomplete pathological or hematological data; ii) stage IV BC at initial diagnosis; iii) failure to complete targeted therapy; iv) failure to undergo surgery as scheduled; v) contraindications to MRI (such as claustrophobia or contrast allergy); and vi) complicated by other primary malignant tumors. The same inclusion and exclusion criteria were applied uniformly to both the retrospective and prospective cohorts.

A total of 2,916 patients with HER2-positive invasive BC were retrospectively screened, 269 of whom met the eligibility criteria and were included for model development and internal validation. Subsequently, 24 patients meeting the same criteria were prospectively enrolled for external validation. The study flowchart is presented in Fig. 1. All patients included were female, and the median age was 48 years (range, 24-73 years). The retrospective cohort comprised 269 female patients, with a median age of 48 years (range, 24-68 years). The prospective cohort included 24 female patients, with a median age of 44 years (range, 29-73 years).

Clinical data collection

Basic clinical features and NAT regimens. Collected clinically relevant variables included sex, age, menstrual status, marital status and TNM stage (based on the 8th edition of the American Joint Committee on Cancer staging manual (21), as well as chemotherapy and targeted therapy regimens. Neoadjuvant chemotherapy regimens in this study primarily included Taxol + carboplatin (21-day cycle, for six cycles) and anthracyclines + cyclophosphamide followed by Taxol (21-day cycle, for eight cycles). Targeted therapy included trastuzumab (Herceptin) alone or dual-target trastuzumab + pertuzumab (HP), administered every 21 days for a duration of 1 year.

Pathological data. Estrogen receptor (ER), progesterone receptor (PR), Ki-67 and HER2 status were assessed using immunohistochemistry on initial biopsy specimens and independently confirmed by two pathologists, which were directly obtained from the original diagnostic pathology reports in the patients' medical records, as assessed by the institutional

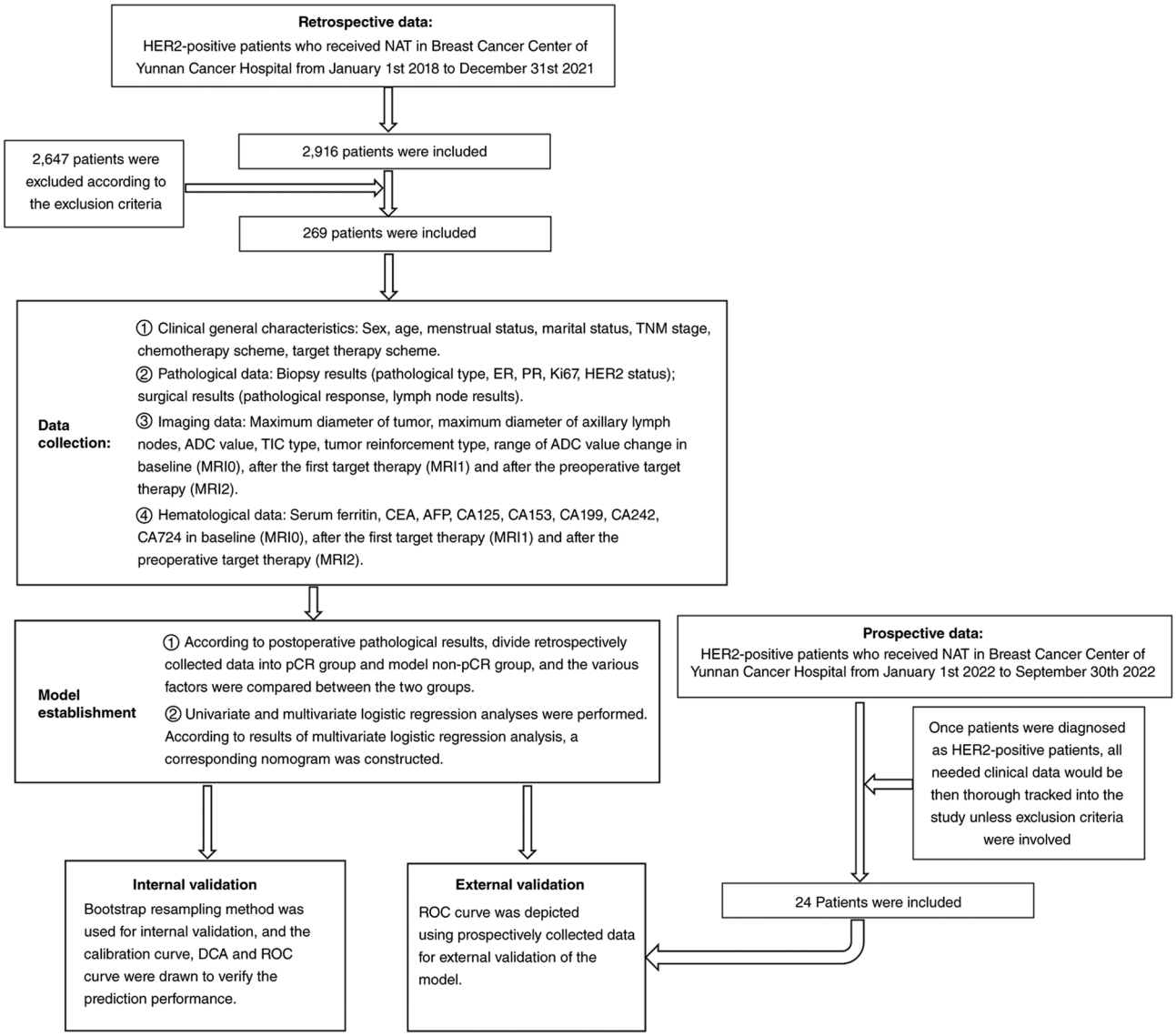

Figure 1. Flowchart of the whole study. A simple and clear flowchart of the whole study to demonstrate how this study was carried out step by step from data collection to model construction and validation. HER2, human epidermal growth factor receptor 2; NAT, neoadjuvant therapy; TNM, Tumor-Node-Metastasis; ER, estrogen receptor; PR, progesterone receptor; ADC, apparent diffusion coefficient; TIC, time intensity curve; MRI, magnetic resonance imaging; CEA, carcinoembryonic antigen; AFP, α-fetoprotein; CA, carbohydrate antigen; pCR, pathological complete response; DCA, decision curve analysis; ROC, receiver operating characteristic.

pathology department. Following completion of NAT, surgical treatment was performed based on patient preference, tumor size and relevant clinical status. pCR was defined as the absence of residual invasive cancer cells in the breast and negative axillary lymph nodes on postoperative pathological evaluation.

Imaging data acquisition. MRI examinations were performed using a Siemens Avanto1.5T system (Siemens AG) with a dedicated four-channel breast coil. Patients were positioned prone with both breasts placed within the coil (head advanced, arms raised and bilateral breasts naturally overhung in the groove of the coil on the surface of the breast). DCE-MRI was conducting using a three-dimensional dynamic imaging sequence (repetition time, 4.43 msec; echo time, 1.5 msec; field of view, 340 mm; slice thickness, 1.7 mm; flip angle, 10°; average acquisition times, once). After an acquisition of pre-contrast images, gadodiamide was administered intravenously at a dose of 0.2 mmol/kg (body weight), and a rate of 2.5 ml/sec followed by seven sequential dynamic enhancement acquisitions (60 sec per phase).

The imaging data collected included the maximum tumor diameter, maximum axillary lymph node diameter, ADC value, TIC type and tumor enhancement type on MRI at baseline before the first NTT (MRI0), after the first NTT (MRI1) and after the last NTT (MRI2). MRI0 data was collected before any invasive procedures such as biopsy, when the tumor remained completely unaltered by any intervention, which denotes the most original state of the disease at the time of initial discovery. The ADC values in MRI0, MRI1 and MRI2 were recorded as ADC0, ADC1 and ADC2, respectively. Relative changes in ADC were calculated as ΔADC1 (ADC1 vs. ADC0), ΔADC2 (ADC2 vs. ADC0) and ΔADC3 (ADC2 vs. ADC1). The TIC types in MRI0, MRI1 and MRI2 were denoted as TIC0, TIC1 and TIC2, respectively.

Hematological data. Serum ferritin (SF), CEA, α-fetoprotein (AFP), CA125, CA153, CA199, CA242 and CA724 were measured using a chemiluminescence immunoassay (Sample source and amount: Fasting venous blood (5 ml) was collected from each patient before treatment. Serum was separated by centrifugation at 1,510 x g for 10 min at room temperature. Assay platform and reagents: The serum levels of SF, CEA, AFP, CA125, CA153, CA199, CA242 and CA724 were measured using a cobas 8000 e801 electrochemiluminescence immunoassay analyzer (Roche Diagnostics) with paired reagent kits (cat. no. 2019062457). All procedures were performed strictly according to the instrument and reagent instructions). Measurements were recorded at baseline (-0), after the first cycle of targeted therapy (-1) and after completion of NAT before surgery (-2).

Construction and validation of nomogram model. Continuous variables with skewed distributions are presented as the median (range), whereas normally distributed variables are expressed as the mean ± standard deviation. Categorical variables are presented as frequency (percentage). Patients were categorized into pCR and non-pCR groups based on postoperative pathological information.

Comparisons between groups were performed using unpaired independent-samples Student's t-test or Levene's test for continuous variables, the rank-sum test for ordinal variables, and Pearson's χ^2 test or Fisher's exact test for categorical variables. For retrospective data, univariate logistic regression analysis was conducted to identify factors associated with pCR after NAT, and variables with P<0.10 were subsequently included in multivariate logistic regression analysis to identify independent predictors. These predictors were used to construct the nomogram.

Internal validation was performed using bootstrap resampling (1,000 iterations). Calibration curves were generated to assess agreement between predicted and observed outcomes. Decision curve analysis (DCA) was conducted to evaluate clinical utility across a range of threshold probabilities. Model discrimination was assessed using receiver operating characteristic (ROC) curves and the area under the ROC curve (AUC), with AUC >0.75 indicating good predictive performance.

External validation was conducted using prospective data, and ROC curves and AUC values were calculated accordingly.

Statistical analysis. Statistical analyses were performed using SPSS 22.0 (IBM Corp.), Graphpad Prism version 7.0 (Dotmatics) and R software (version 4.1.2; https://www.r-project.org/). R packages used included rms, pROC, rmda and caret. Two-sided P<0.05 was considered to indicate a statistically significant difference.

Results

Significant differences in the distribution of four basic clinical characteristics in the comparison between pCR and non-pCR groups in retrospective data. A total of 269 patients were included in the retrospective cohort. All patients were female, married and diagnosed with invasive ductal carcinoma. Significant differences were observed in four clinical characteristics between the pCR group and non-pCR groups. Regarding tumor burden, T stage was predominantly T2 in both groups; however, the proportion of T2 tumors was significantly higher in the pCR group than in the non-pCR group (68.32 vs. 50.00%). Similarly, patients in the pCR group were more frequently classified as early to mid-stage (2A-3A), whereas those in the non-pCR group were more often in more advanced stages (2B-3B). In terms of hormone receptor expression, the proportions of ER-positive (48.15%) and PR-positive (68.52%) tumors were higher in the non-pCR group than in the pCR group. Regarding the NAT regimen, anthracycline-based chemotherapy and dual-target therapy with HP were the main treatment approaches in both groups (Table I).

In total, 14 basic clinical characteristics were compared. No significant differences were observed between the pCR and non-pCR groups in terms of age, sex, menstrual status, marital status, pathological type, N stage, Ki-67 expression, targeted therapy regimen, chemotherapy regimen, or number of postoperative pathological axillary lymph nodes. However, significant differences were found in T stage, overall TNM stage, ER expression and PR expression (Table I). Specifically, lower T stage, earlier TNM comprehensive stage, and negative ER/PR expression were associated with a higher pCR rate.

Lack of significant differences in the distribution of basic clinical characteristics in the comparison between pCR and non-pCR groups in prospective data. A total of 24 patients with HER2-positive BC were prospectively enrolled as the external validation cohort. The median age in the prospective data was 48.5 years in the pCR group and 40.5 years in the non-pCR group. All of these patients were female, married and had invasive ductal carcinoma. No significant differences were observed in the distribution of the 14 basic clinical characteristics between the two groups (Table II). This lack of significance may be related to the small sample size of the cohort (n=24) limiting statistical power, and the relatively homogeneous baseline characteristics of the prospectively enrolled patients.

Comparison of MRI findings between the pCR and non-pCR groups in the retrospective cohort

MRI0 data. Before NTT, the mean maximum tumor diameter was significantly smaller in the pCR group than that in the non-pCR group. The mean ADC values were ~0.7 in both groups, with no significant difference. In >60% of patients in both groups, the main TIC pattern was the inflow-outflow type (Table III).

MRI1 data. After the first targeted therapy cycle, significant differences in MRI parameters were observed between the two groups. The maximum tumor diameter decreased in both groups and was significantly smaller in the pCR group than that in the non-pCR group (2.217±1.307 vs. 3.516±2.179 cm). The reduction in tumor diameter was greater in the pCR group (41.287%) than in the non-pCR group (23.298%) (Table IV).

The mean ADC1 value in the pCR group was significantly different from that in the non-pCR group. ADC values increased in both groups compared with baseline. The increase in ADC1 relative to ADC0 was greater in the pCR group (28.919%) than in the non-pCR group ΔADC1 (20.384%). In addition, the main TIC type in the pCR group changed from

Table I. Basic clinical characteristic comparison between the pCR and non-pCR groups in retrospective data.

Characteristics	pCR group	Non-pCR group	t/χ^2/Z value	P-value
Age, years[a]	49 (24-68)	46 (27-65)	1.242	0.216
Sex, n (%)			0.000	1.000
Female	161 (100.00)	108 (100.00)		
Male	0 (0.00)	0 (0.00)		
Menstrual status, n (%)			2.226	0.136
Pre-menopausal	79 (49.07)	63 (58.33)		
After menopause	82 (50.93)	45 (41.67)		
Marital status, n (%)			0.000	1.000
Unmarried	0 (0.00)	0 (0.00)		
Married	161 (100.00)	108 (100.00)		
T stage, n (%)			-3.195	0.001[b]
1	6 (3.73)	4 (3.70)		
2	110 (68.32)	54 (50.00)		
3	29 (18.01)	23 (21.30)		
4	16 (9.94)	27 (25.00)		
N stage, n (%)			-1.204	0.229
0	21 (13.04)	9 (8.33)		
1	101 (62.73)	67 (62.04)		
2	31 (19.25)	29 (26.85)		
3	8 (4.97)	3 (2.78)		
TNM stage, n (%)			-2.571	0.010[b]
2A	19 (11.80)	9 (8.33)		
2B	78 (48.45)	40 (37.04)		
3A	42 (26.09)	30 (27.78)		
3B	14 (8.70)	26 (24.07)		
3C	8 (4.97)	3 (2.78)		
Pathological type, n (%)			0.000	1.000
Invasive ductal carcinoma	161 (100.00)	108 (100.00)		
Other types	0 (0.00)	0 (0.00)		
ER status, n (%)			5.777	0.016[b]
Positive	54 (33.54)	52 (48.15)		
Negative	107 (66.46)	56 (51.85)		
PR status, n (%)			7.125	0.008[b]
Positive	84 (52.17)	74 (68.52)		
Negative	77 (47.83)	34 (31.48)		
Ki67[c]	39.690±17.845	37.900±20.500	0.758	0.449
Target therapy scheme, n (%)			3.503	0.061
Herceptin (trastuzumab)	37 (22.98)	36 (33.33)		
Herceptin (trastuzumab) + pertuzumab	124 (77.02)	72 (66.67)		
Chemotherapy scheme, n (%)			0.157	0.692
Taxol + carboplatin	65 (40.37)	41 (37.96)		
Anthracyclines + cyclophosphamide followed by Taxol	96 (59.63)	67 (62.04)		
Number of postoperative axillary lymph nodes[c]	16.660±5.237	16.730±5.779	-0.098	0.922

[a]Data are presented as the median (range). [b]P<0.05. [c]Data are presented as the mean ± standard deviation. pCR, pathological complete response; TNM, Tumor-Node-Metastasis; ER, estrogen receptor; PR, progesterone receptor.

Table II. Basic clinical characteristics comparison between the pCR and non-pCR groups in prospective data.

Characteristics	pCR group	Non-pCR group	t/χ^2/Z value	P-value
Age, years[a]	48.5 (29-73)	40.5 (35-52)	1.565	0.132
Sex, n (%)			0.000	1.000
Female	16 (100.00)	8 (100.00)		
Male	0	0		
Menstrual status, n (%)			-[b]	0.178
Pre-menopausal	8 (50.00)	7 (87.50)		
After menopause	8 (50.00)	1 (12.50)		
Marital status, n (%)			0.000	1.000
Unmarried	0	0		
Married	16 (100.00)	8 (10.00)		
T stage, n (%)			-0.283	0.777
1	2 (12.50)	0		
2	9 (56.25)	6 (75.00)		
3	2 (12.50)	0		
4	3 (18.75)	2 (25.00)		
N stage, n (%)			-0.245	0.806
0	0	2 (25.00)		
1	8 (50.00)	6 (75.00)		
2	7 (43.75)	0		
3	1 (6.25)	0		
TNM stage, n (%)			-1.403	0.161
2A	1 (6.25)	2 (25.00)		
2B	5 (31.25)	4 (50.00)		
3A	6 (37.50)	0		
3B	3 (18.75)	2 (25.00)		
3C	1 (6.25)	0		
Pathological type, n (%)			0.000	1.000
Invasive ductal carcinoma	16 (100.00)	8 (100.00)		
Other types	0	0		
ER status, n (%)			-[b]	0.099
Positive	4 (25.00)	5 (62.50)		
Negative	12 (75.00)	3 (37.50)		
PR status, n (%)			-[b]	0.099
Positive	4 (25.00)	5 (62.50)		
Negative	12 (75.00)	3 (37.50)		
Ki67[c]	30.000±9.832	28.125±15.338	0.365	0.719
Target therapy scheme, n (%)			-[b]	0.647
Herceptin (trastuzumab)	4 (25.00)	3 (37.50)		
Herceptin (trastuzumab) + pertuzumab	12 (75.00)	5 (62.50)		
Chemotherapy scheme, n (%)			-[b]	0.289
Taxol + carboplatin	14 (87.50)	5 (62.50)		
Anthracyclines + cyclophosphamide followed by Taxol	2 (12.50)	3 (37.50)		
Number of postoperative axillary lymph nodes[c]	16.630±6.407	14.630±6.301	-0.725	0.476

[a]Data are presented as the median (range). [b]-means no test statistic from Fisher's exact test. [c]Data are presented as the mean ± standard deviation. pCR, pathological complete response; TNM, Tumor-Node-Metastasis; ER, estrogen receptor; PR, progesterone receptor.

Table III. Comparison of MRI0 data between pCR group and non-pCR groups.

MRI0	pCR group	Non-pCR group	t/χ^2/Z value	P-value
Maximum diameter of tumor, cm[a]	3.776±1.753	4.584±2.249	-3.147	0.002[b]
Maximum diameter of axillary lymph nodes, cm[a]	1.521±1.180	1.293±0.950	1.671	0.096
ADC0 (x10^{-3} mm^2/sec)[a]	0.746±0.151	0.716±0.134	1.710	0.088
MRI0 TIC0 type, n (%)			1.221	0.543
Inflow-inflow	5 (3.11)	2 (1.85)		
Inflow-platform	57 (35.40)	33 (30.56)		
Inflow-outflow	99 (61.49)	73 (67.59)		
Reinforcement-type, n (%)			0.260	0.878
No reinforcement	9 (5.59)	7 (6.48)		
Reinforcement	146 (90.68)	98 (90.74)		
Uneven reinforcement	6 (3.73)	3 (2.78)		

[a]Data are presented as the mean ± standard deviation. [b]P<0.05. pCR, pathological complete response; MRI0, magnetic resonance imaging data at baseline; ADC0, apparent diffusion coefficient at baseline; TIC0, time intensity curve at baseline.

Table IV. MRI1 data comparison between the pCR and non-pCR groups.

MRI1	pCR group	Non-pCR group	t/χ^2/Z value	P-value
Maximum diameter of tumor, cm[a]	2.217±1.307	3.516±2.179	-5.560	<0.001[b]
Maximum diameter of axillary lymph nodes, cm[a]	0.784±0.803	0.823±0.691	-0.409	0.683
ADC1 (x10^{-3} mm^2/sec)[a]	1.035±0.281	0.919±0.228	3.721	<0.001[b]
MRI1 TIC1 type, n (%)			27.886	<0.001[b]
Inflow-inflow	41 (25.47)	12 (11.11)		
Inflow-platform	83 (51.55)	38 (35.19)		
Inflow-outflow	37 (22.98)	58 (53.70)		
Reinforcement type, n (%)			0.254	0.881
No reinforcement	14 (8.70)	9 (8.33)		
Reinforcement	144 (89.44)	96 (88.89)		
Uneven reinforcement	3 (1.86)	3 (2.78)		
ΔADC1, %	28.919±31.935	20.384±22.760	2.558	0.011[b]

[a]Data are presented as the mean ± standard deviation. [b]P<0.05. pCR, pathological complete response; MRI1, magnetic resonance imaging data after the first cycle of targeted therapy; ADC1, apparent diffusion coefficient after the first cycle of targeted therapy; TIC1, time intensity curve after the first cycle of targeted therapy; ΔADC1, calculated change in ADC value (ADC1 vs. ADC0).

inflow-outflow to inflow-platform, whereas the main TIC type in the non-pCR group remained as inflow-outflow (Table IV).

MRI2 data. After 4-6 cycles of preoperative NAT, the maximum tumor diameter was further reduced in both groups, and the tumor diameter in the pCR group remained significantly smaller than that in the non-pCR group. In the pCR group, the ADC2 value increased to 1.222±0.256 (x10^{-3} mm^2/sec), which was 18.617 and 47.536% higher than the ADC1 and ADC0 values, respectively. In the non-pCR group, the average value of ADC2 increased to 0.944±0.264 (x10^{-3} mm^2/sec), which was 2.470 and 22.855% higher than those of the ADC1 and ADC0 values, respectively. ADC2, ΔADC2 and ΔADC3 were all significantly higher in the pCR group than those in the non-pCR group. The main TIC type in the pCR group further changed to the inflow-inflow type (74.5%), whereas the main TIC type in the non-pCR group changed from the inflow-outflow at MRI0 and MRI1 to the inflow-platform at MRI2 (Table V).

Hematological characteristics comparison between pCR and non-pCR groups in the retrospective cohort. At baseline, SF0 was significantly higher and CEA0 was significantly lower in the pCR group than those values in the non-pCR group. After the first targeted therapy cycle, only CEA1 differed significantly between the two groups, and the CEA showed continuous downward trend from baseline to the last time point in both groups. After the last preoperative targeted therapy, CEA2, AFP2 and CA153-2 were significantly lower in the pCR group than in the non-pCR group. No significant differences were found in CA125, CA19-9, CA242 and CA724 between the two groups (Table VI).

Table V. Comparison of MRI2 data between the pCR and non-pCR groups.

MRI2	pCR group	Non-pCR group	t/χ^2/Z value	P-value
Maximum diameter of tumor, cm[a]	1.515±1.182	2.517±1.860	-4.965	<0.001[b]
Maximum diameter of axillary lymph nodes, cm[a]	0.442±0.436	0.469±0.501	-0.472	0.637
ADC2 (x10^{-3} mm^2/sec)[a]	1.222±0.256	0.944±0.264	8.613	<0.001[b]
MRI2 TIC2 type, n (%)				<0.001[b]
Inflow-inflow	120 (74.53)	22 (20.37)	77.505	
Inflow-platform	29 (18.01)	51 (47.22)		
Inflow-outflow	12 (7.45)	35 (32.41)		
Type of reinforcement, n (%)			1.715	0.424
No reinforcement	17 (10.56)	11 (10.19)		
Reinforcement	141 (87.58)	92 (85.19)		
Uneven reinforcement	3 (1.86)	5 (4.63)		
ΔADC2, %	47.536±30.597	22.855±25.765	7.136	<0.001[b]
ΔADC3, %	18.617±29.274	2.470±23.459	4.792	<0.001[b]

[a]Data are presented as the mean ± standard deviation. [b]P<0.05. pCR, pathological complete response; MRI2, magnetic resonance imaging data after completion of neoadjuvant therapy before surgery; ADC2, apparent diffusion coefficient after completion of neoadjuvant therapy before surgery; TIC2, time intensity curve after completion of neoadjuvant therapy before surgery; ΔADC2, calculated change in ADC value (ADC2 vs. ADC0); ΔADC3, calculated change in ADC value (ADC2 vs. ADC1).

Univariate logistic regression analysis of retrospective data. Univariate logistic regression analysis revealed that TNM stage 2A (vs. 3B), ER status, PR status, maximum diameter (in MRI0, MRI1, and MRI2), TIC inflow to inflow type in MRI1 (vs. inflow to outflow type), TIC inflow to inflow type in MRI2 (vs. inflow to outflow type and vs. inflow to platform type) ADC1, ADC2, ΔADC1, ΔADC2, ΔADC3, SF0, CEA-0, CEA1, CEA-2, AFP-0, AFP-2 and CA153-2 were predictive factors for pCR (Table VII).

Multivariate logistic regression analysis of retrospective data. Variables identified as significant in the univariate logistic regression analysis of retrospective data were engaged in the multivariate logistic regression analysis. To reduce the omission of potentially important factors due to interaction, variables with P<0.10 were identified as predictors. Prior to multivariate logistic regression, multicollinearity among the included variables was assessed using variance inflation factors (VIFs). All VIF values were <5, indicating no significant collinearity. The results showed that pCR was more likely to occur in patients with negative PR, higher ADC2 at MRI2, inflow-inflow type in TIC2, greater ΔADC2, greater ΔADC3, and lower CEA-0, CEA-1 and CA153-2 (Table VIII).

Development and evaluation of the nomogram of the prediction model

Construction of the pCR prediction nomogram. Based on the multivariate logistic regression analysis of the retrospective data, eight predictive factors were selected from all included variables. The multivariate prediction model was visualized, and the nomogram was constructed using R software (Fig. 2).

Internal validation of the pCR prediction model. The nomogram was internally validated using the bootstrap method. The Hosmer-Lemeshow test indicated good fit of the prediction model (P=0.453). A calibration curve was then constructed according to the relationship between the predicted results and the actual outcomes, showing close agreement between the model performance curve and the diagonal reference line. This indicated good consistency between the predicted and observed pCR outcomes (Fig. 3).

The DCA curve further showed that the prediction model provided net benefit across a threshold probability range of 0-80% (Fig. 4). ROC analysis yielded an AUC of 0.886, with an optimal cut-off value of 0.605, sensitivity of 0.822 and specificity of 0.818, indicating good predictive performance and accuracy (Fig. 5).

External validation of the pCR prediction model. A total of 24 patients with HER2-positive BC were prospectively included as the external validation cohort, and an ROC curve was generated for external validation. The AUC value was 0.961 (P=0.001), with an optimal cut-off value of 0.854, sensitivity of 1.000 and specificity of 0.875, indicating good predictive performance and high accuracy in the external validation cohort (Fig. 6).

Discussion

pCR is an important endpoint in the management of HER2-positive BC, and pCR rates after first-line NAT scheme are relatively high in patients with this subtype (22,23). Previous studies, including the NeoSphere trial, demonstrated that patients achieving a pCR had improved 5-year progression-free survival rates compared with those without a pCR (85 vs. 76%; HR, 0.54; 95% CI, 0.29-1.00) (9). Similar findings were reported in the PEONY trial, in which the pCR group showed a higher 5-year disease-free survival rate than the non-pCR group (91.5 vs. 82.1%) (24). These findings have led some investigators to propose pCR as a surrogate endpoint for prognosis in patients

Table VI. Tumor marker comparison between the pCR and non-pCR groups in retrospective data.

Tumor markers	pCR group	Non-pCR group	$t/\chi^2/Z$ value	P-value
SF				
SF0	295.994±164.773	279.620±328.425	2.068	0.041[a]
SF1	302.903±248.534	277.180±256.492	0.765	0.445
SF2	268.724±269.541	260.738±224.678	0.240	0.810
CEA				
CEA0	4.110±6.206	6.298±8.923	2.175	0.031[a]
CEA1	2.361±1.487	4.070±3.902	4.326	<0.001[a]
CEA2	2.041±1.213	2.693±1.602	3.776	<0.001[a]
AFP				
AFP0	4.525±2.697	3.802±2.300	2.129	0.034
AFP1	3.526±2.264	3.658±2.078	0.440	0.660
AFP2	3.186±2.173	3.821±2.347	2.083	0.038[a]
CA125				
CA125-0	19.397±15.353	18.621±9.759	0.466	0.642
CA125-1	15.983±8.139	16.790±7.732	0.812	0.417
CA125-2	13.683±5.758	14.923±7.463	1.460	0.146
CA153				
CA153-0	16.714±12.249	17.442±16.418	0.416	0.678
CA153-1	19.068±11.397	21.599±15.404	1.547	0.123
CA153-2	17.026±7.557	20.117±9.629	2.801	0.006[a]
CA199				
CA199-0	14.942±10.995	12.799±10.144	1.481	0.140
CA199-1	14.300±11.163	13.946± 8.874	0.248	0.804
CA199-2	14.538±10.130	14.053±10.647	0.344	0.732
CA242				
CA242-0	8.507±8.464	6.844±5.425	1.644	0.102
CA242-1	8.217±7.216	7.149±5.492	1.172	0.242
CA242-2	8.822±7.203	8.203±7.879	0.606	0.545
CA724				
CA724-0	6.913±11.026	6.468±9.677	0.288	0.774
CA724-1	8.025±9.438	7.806±20.223	0.106	0.916
CA724-2	9.257±12.741	9.142±17.916	0.055	0.956

[a]P<0.05. Data are presented as the mean ± standard deviation. pCR, pathological complete response; SF, serum ferritin; CEA, carcinoembryonic antigen; AFP, α-fetoprotein; CA, carbohydrate antigen; suffix '-0' denoted data at baseline; suffix '-1' denoted data after the first cycle of targeted therapy; suffix '-2' denoted data after completion of neoadjuvant therapy before surgery.

with HER2-positive BC (25-27). However, improving outcomes in HER2-positive BC requires not only advances in targeted therapies but also accurate monitoring of treatment response. Therefore, there is an increasing need to develop reliable predictive tools, such as nomograms, based on clinically available auxiliary examination indicators to estimate pCR.

In the present study, a nomogram for pCR incorporating MRI features and tumor markers was developed to predict pCR. The model indicated that pCR was more likely to occur when PR was negative, ADC2 was higher, TIC2 was of inflow-inflow type, ΔADC2 and ΔADC3 were larger, and CEA-0, CEA-1 and CA153-2 were lower. The further internal and external validation confirmed that the nomogram had good predictive performance for pCR patients with HER2-positive BC.

HR status plays an important part in the prognosis, diagnosis and treatment of BC (28). HR status determines the molecular subtype and guides the use of endocrine therapy, and is also associated with response to NAT (29-30). In the present study, PR status was associated with neoadjuvant pCR, with a higher probability of achieving a pCR observed in patients with PR-negative tumors (OR, 0.543; 95% CI, 0.330-0.896; P=0.017). Previous studies have similarly reported that patients with the HR-negative subtype are more likely to achieve a pCR than their HR-positive counterparts (P=0.011) (31), particularly in younger patients with HER2-positive BC and lower tumor burden who receive standardized HER2-targeted therapy (32). Potential mechanisms include the role of PR in regulating

Table VII. Univariate logistics regression analysis of all factors in retrospective data.

Characteristics	Univariate logistics regression analysis				
	β	P-value	OR	95% CI	
Age	0.017	0.215	1.017	0.990	1.045
Menstrual conditions	0.374	0.136	0.688	0.421	1.125
T stage					
T1-T2	0.306	0.646	1.358	0.368	5.015
T1-T3	0.174	0.805	0.841	0.212	3.336
T1-T4	0.929	0.196	0.395	0.097	1.615
N stage					
N0-N1	0.437	0.308	0.646	0.279	1.496
N0-N2	0.781	0.100	0.458	0.181	1.162
N0-N3	0.134	0.865	1.143	0.245	5.329
TNM stage					
2A-2B	0.079	0.860	0.924	0.383	2.227
2A-3A	0.411	0.382	0.663	0.264	1.666
2A-3B	1.366	0.009[a]	0.255	0.091	0.711
2A-3C	0.234	0.767	1.263	0.269	5.927
Age	0.017	0.215	1.017	0.990	1.045
ER status	0.610	0.017[a]	0.543	0.330	0.896
PR status	0.691	0.008[a]	0.501	0.301	0.835
Ki67	0.005	0.448	1.005	0.992	1.018
Target scheme	0.516	0.062	1.676	0.974	2.884
Chemotherapy scheme	0.101	0.692	1.106	0.671	1.824
Number of postoperative axillary lymph nodes	0.002	0.921	0.998	0.954	1.043
Maximum diameter of MRI0 tumor, cm	0.206	0.002[a]	0.814	0.716	0.925
MRI0 maximum diameter of axillary lymph nodes, cm	0.197	0.098	1.218	1.218	0.964
MRI0 ADC0 ($x10^{-3}$ mm^2/sec)	1.507	0.090	4.515	0.791	25.777
MRI0 TIC0 type					
Inflow to inflow-inflow to platform	0.370	0.669	0.691	0.127	3.763
Inflow to inflow-inflow to outflow	0.612	0.472	0.542	0.102	2.874
MRI0 reinforcement type					
No reinforcement-reinforcement	0.147	0.777	1.159	0.418	3.215
No reinforcement-uneven reinforcement	0.442	0.611	1.556	0.284	8.531
Maximum diameter of MRI1 tumor, cm	0.460	<0.001[a]	0.631	0.531	0.751
MRI1 maximum diameter of axillary lymph nodes, cm	0.067	0.682	0.935	0.679	1.288
MRI1 ADC1 ($x10^{-3}$ mm^2/sec)	1.904	0.001[a]	6.710	2.239	20.115
MRI1 TIC1 type					
Inflow to inflow-inflow to platform	0.447	0.242	0.639	0.302	1.352
Inflow to inflow-inflow to outflow	1.678	<0.001[a]	0.187	0.087	0.401
MRI1 reinforcement type					
No reinforcement-reinforcement	-0.036	0.935	0.964	0.401	2.316
No reinforcement-uneven reinforcement	-0.442	0.632	0.643	0.106	3.913
Maximum diameter of MRI2 tumor, cm	0.489	<0.001[a]	0.613	0.499	0.754
MRI2 maximum diameter of axillary lymph nodes, cm	0.127	0.636	0.880	0.520	1.491
MRI2 ADC2 ($x10^{-3}$ mm^2/sec)	4.516	<0.001[a]	91.446	25.140	332.628
MRI2 TIC2					
Inflow to inflow-inflow to platform	2.261	<0.001[a]	0.104	0.055	0.198
Inflow to inflow-inflow to outflow	2.767	<0.001[a]	0.063	0.028	0.140
MRI2 reinforcement type					
No reinforcement-reinforcement	-0.008	0.984	0.992	0.444	2.213

Table VII. Continued.

Characteristics	Univariate logistics regression analysis				
	β	P-value	OR	95% CI	
No reinforcement-uneven reinforcement	-0.946	0.252	0.388	0.077	1.962
ΔADC1	1.127	0.019[a]	3.085	1.200	7.934
ΔADC2	3.347	<0.001[a]	28.406	9.279	86.964
ΔADC3	2.339	<0.001[a]	10.370	3.564	30.175
SF					
SF0	0.001	0.025[a]	0.999	0.998	1.000
SF1	0.000	0.446	1.000	0.998	1.001
SF2	0.000	0.810	1.000	0.999	1.001
CEA					
CEA-0	0.004	0.039[a]	0.957	0.918	0.998
CEA-1	0.272	<0.001[a]	0.762	0.673	0.864
CEA-2	0.336	<0.001[a]	0.715	0.594	0.861
AFP					
AFP-0	0.117	0.036[a]	1.124	1.007	1.253
AFP-1	0.027	0.659	0.973	0.861	1.099
AFP-2	0.125	0.043[a]	0.883	0.782	0.996
CA125					
CA125-0	0.004	0.641	1.004	0.986	1.023
CA125-1	0.013	0.417	0.987	0.958	1.018
CA125-2	0.029	0.129	0.971	0.935	1.008
CA153					
CA153-0	0.004	0.678	0.996	0.979	1.014
CA153-1	0.015	0.134	0.985	0.967	1.005
CA153-2	0.043	0.005[a]	0.958	0.930	0.987
CA199					
CA199-0	0.020	0.143	1.020	0.993	1.048
CA199-1	0.003	0.803	1.003	0.977	1.030
CA199-2	0.005	0.730	1.005	0.979	1.031
CA242					
CA242-0	0.034	0.107	1.034	0.993	1.077
CA242-1	0.025	0.243	1.026	0.983	1.070
CA242-2	0.011	0.544	1.011	0.975	1.050
CA724					
CA724-0	0.004	0.773	1.004	0.976	1.033
CA724-1	0.001	0.916	1.001	0.981	1.021
CA724-2	0.001	0.956	1.001	0.982	1.019

[a]P<0.05. OR, odds ratio; CI, confidence interval; SF, serum ferritin; CEA, carcinoembryonic antigen; AFP, α-fetoprotein; CA, carbohydrate antigen; TNM, Tumor-Node-Metastasis; ER, estrogen receptor; PR, progesterone receptor; ADC, apparent diffusion coefficient; MRI, magnetic resonance imaging; TIC, time intensity curve; suffix '-0' denoted data at baseline; suffix '-1' denoted data after the first cycle of targeted therapy; suffix '-2' denoted data after completion of neoadjuvant therapy before surgery; ΔADC1, calculated change in ADC value (ADC1 vs. ADC0); ΔADC2, calculated change in ADC value (ADC2 vs. ADC0); ΔADC3, calculated change in ADC value value (ADC2 vs. ADC1).

growth factor-related signaling pathways and interactions between HR and HER2 signaling during dual-target therapy (33), as well as HR-mediated promotion of tumor cell proliferation and potential induction of trastuzumab resistance (34).

In recent years, the role of imaging data in predicting the response to NAT has also been increasingly recognized, and MRI is considered one of the most accurate imaging modalities for the evaluation of breast lesions (35). In the present study, both morphological and functional imaging

Table VIII. Multivariate logistic regression analysis.

Characteristics	Multivariate logistic regression analysis				
	β	P-value	OR	95% CI	
TNM stage					
2A-2B	0.257	0.714	1.293	0.328	5.099
2A-3A	0.124	0.880	1.132	0.229	5.597
2A-3B	0.008	0.993	1.008	0.147	6.924
2A-3C	0.240	0.858	1.272	0.091	17.698
ER status	0.390	0.464	0.677	0.238	1.924
PR status	0.962	0.095[a]	0.382	0.124	1.183
Maximum diameter of MRI0 tumor, cm	0.236	0.291	1.267	0.816	1.965
Maximum diameter of MRI1 tumor, cm	0.359	0.188	0.699	0.410	1.192
MRI1 ADC1 ($x10^{-3}$ mm^2/sec)	0.753	0.685	2.124	0.056	80.899
MRI1 TIC1 type					
Inflow to inflow-inflow to platform	0.071	0.913	1.074	0.300	3.842
Inflow to inflow-inflow to outflow	1.134	0.856	0.857	0.207	3.698
Maximum diameter of MRI2 tumor, cm	0.179	0.515	1.196	0.698	2.052
MRI2 ADC2 ($x10^{-3}$ mm^2/sec)	2.122	0.023[a]	8.349	1.344	51.856
MRI2 TIC2 type					
Inflow to inflow-inflow to platform	2.157	<0.001[a]	0.116	0.038	0.351
Inflow to inflow-inflow to outflow	3.184	<0.001[a]	0.041	0.009	0.190
ΔADC1 (%)	0.360	0.833	0.697	0.025	19.823
ΔADC2 (%)	3.347	0.023[a]	28.406	9.279	86.964
ΔADC3 (%)	2.339	<0.001[a]	10.370	3.564	30.175
SF					
SF-0	0.001	0.197	0.999	0.998	1.000
CEA					
CEA-0	0.004	0.078[a]	0.957	0.918	0.998
CEA-1	0.272	0.039[a]	0.762	0.673	0.864
CEA-2	0.336	0.177	0.715	0.594	0.861
AFP					
AFP-0	0.027	0.546	0.973	0.861	1.099
AFP-2	0.125	0.201	0.883	0.782	0.996
CA153					
CA153-2	0.043	0.040[a]	0.958	0.930	0.987

[a]P<0.10. OR, odds ratio; CI, confidence interval; SF, serum ferritin; CEA, carcinoembryonic antigen; AFP, α-fetoprotein; CA, carbohydrate antigen; TNM, Tumor-Node-Metastasis; ER, estrogen receptor; PR, progesterone receptor; ADC, apparent diffusion coefficient; MRI, magnetic resonance imaging; TIC, time intensity curve; suffix '-0' denoted data at baseline; suffix '-1' denoted data after the first cycle of targeted therapy; suffix '-2' denoted data after completion of neoadjuvant therapy before surgery; ΔADC1, calculated change in ADC value (ADC1 vs. ADC0); ΔADC2, calculated change in ADC value (ADC2 vs. ADC0); ΔADC3, calculated change in ADC value value (ADC2 vs. ADC1).

parameters, including the maximum tumor diameter, maximum axillary lymph node diameter, TIC type and ADC value, were assessed at three time points. Before NAT, the maximum tumor diameter was associated with prognosis, with larger tumors diameter showing a lower probability of achieving a pCR. This finding is consistent with those of a previous study (36) and further supports the importance of tumor size in predicting NAT efficacy and informing surgical planning (37).

The TIC reflects changes in contrast enhancement on DCE-MRI. Malignant lesions typically show higher vascular density, greater vascular permeability and a larger extravascular space, resulting in a more rapid contrast agent flow rate. According to the Kulh criteria (38), malignant tumors usually present with a type III curve, namely an inflow-outflow pattern. In the present study, the predominant TIC pattern at baseline was inflow-outflow in both the pCR and the non-pCR groups. However, after NTT, as the tumor gradually regressed

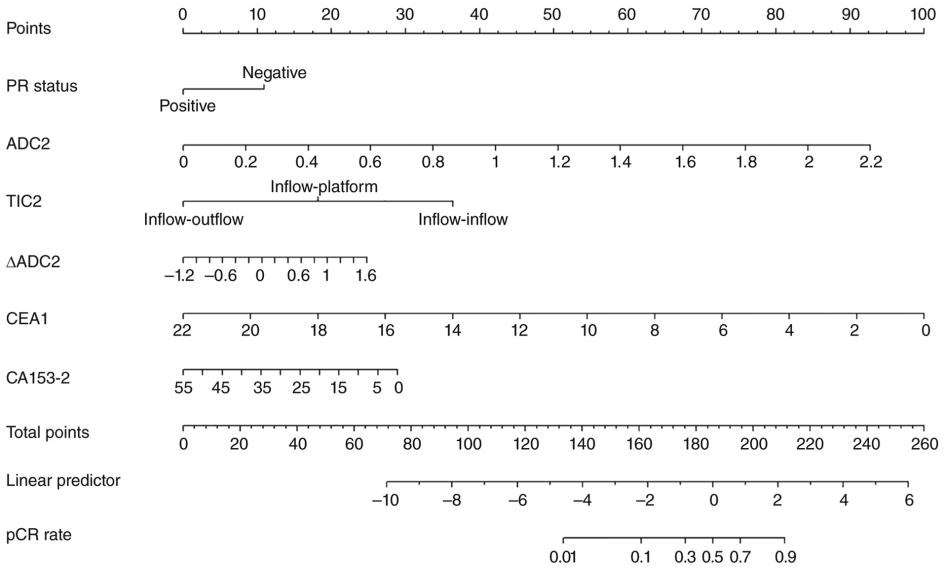

Figure 2. Nomogram to predict the probability of pCR in human epidermal growth factor receptor 2-positive breast cancer after neoadjuvant targeted therapy A predictive model based on the multivariate analysis of the present study from the retrospectively collected data. According to the nomogram, each screened predictor was projected to the scale above the nomogram to calculate the individual score of each factor, and the total score was calculated after adding the individual scores. The corresponding prediction probability was then obtained according to the relationship between the total score and pCR in the nomogram. pCR, pathological complete response; PR, progesterone receptor; ADC, apparent diffusion coefficient; TIC, time intensity curve; CEA, carcinoembryonic antigen; CA, carbohydrate antigen; ADC2, ADC after completion of neoadjuvant therapy before surgery; TIC2, TIC type after completion of neoadjuvant therapy before surgery; ΔADC2, calculated change in ADC value (ADC2 vs. ADC0); CEA1, CEA after the first cycle of targeted therapy; CA153-2, CA153 after completion of NAT before surgery.

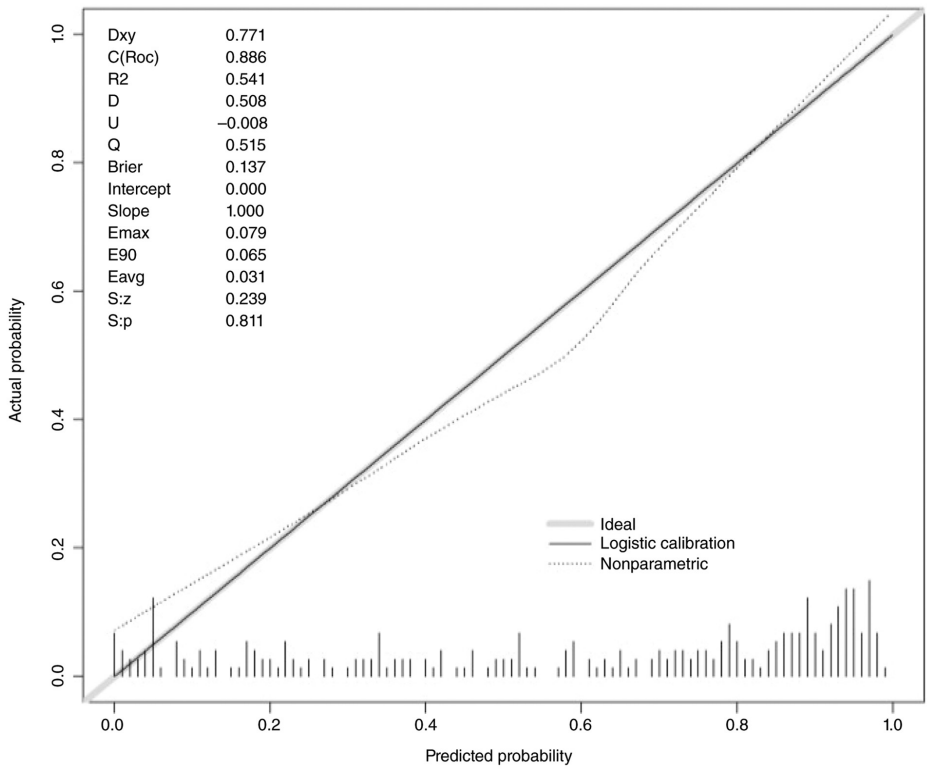

Figure 3. Calibration curve of the constructed predictive model from internal validation data. As part of the internal validation, the calibration curve was drawn according to the relationship between the prediction results and the actual situation. The calibration curve showed that the dotted line and diagonal line of the model were coincident, indicating that the nomogram had good consistency between the prediction of pCR and the actual occurrence of pCR, and the prediction ability was good. The following internal validation metrics were obtained: Somer's Dxy rank correlation was 0.771; concordance index (C-index) was 0.886 (indicating good discrimination); R2 was 0.541 (indicating moderate explanatory power); Brier score was 0.137 (<0.25, indicating acceptable overall prediction accuracy); calibration intercept was 0.000 (ideal value was 0, indicating no systematic over- or under-estimation); calibration slope was 1.000 (ideal value was 1, indicating perfect calibration slope); maximum calibration error (Emax) was 0.079; 90th percentile calibration error (E90) was 0.065; mean absolute calibration error (Eavg) was 0.031 (all indicating small prediction errors). The Spiegelhalter's Z-test statistic (S:z) was 0.239 (P=0.811, S:p), indicating no significant deviation from perfect calibration. Collectively, these metrics demonstrate that the nomogram has good calibration and predictive performance. pCR, pathological complete response.

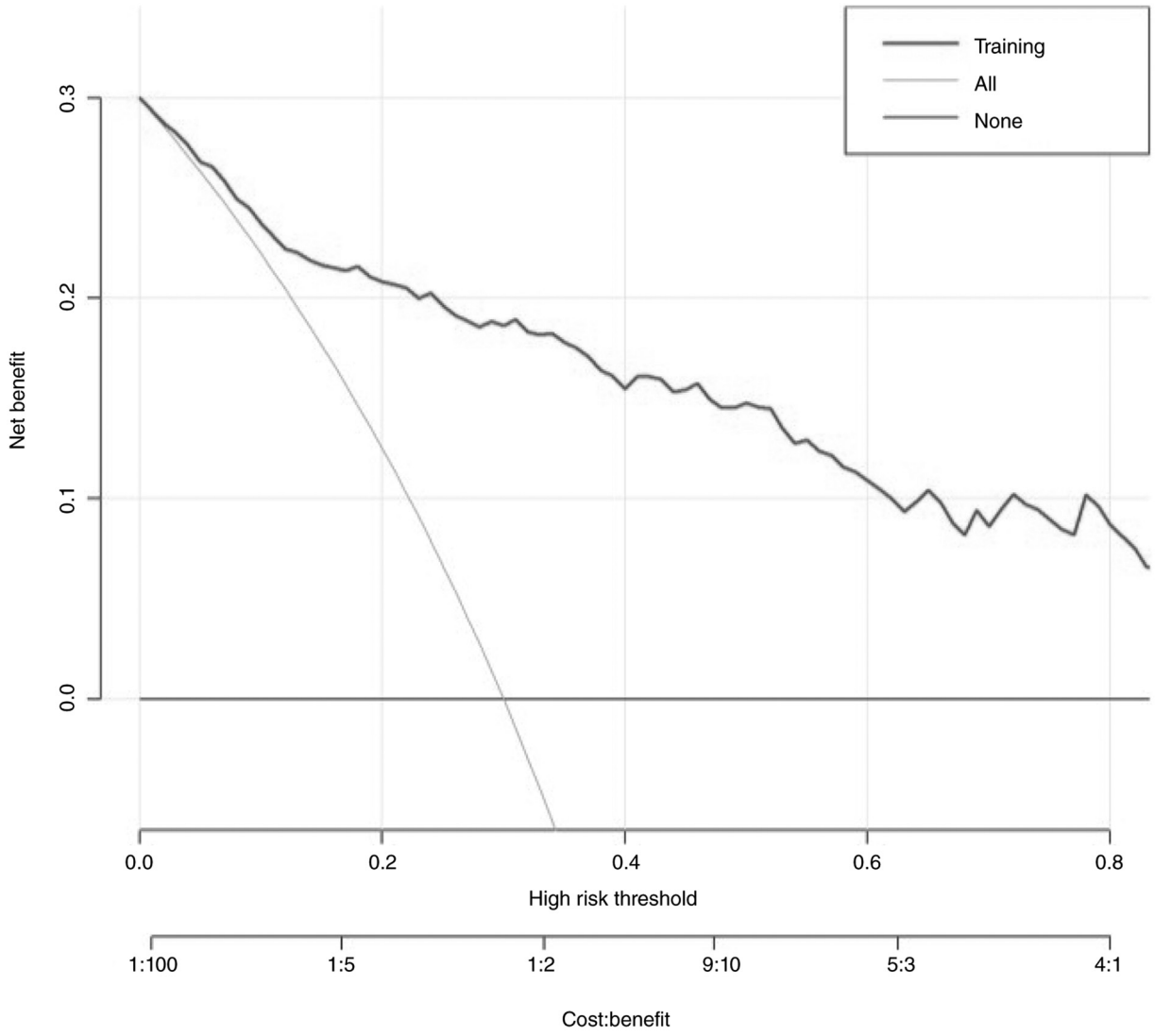

Figure 4. DCA curve of the predictive model from internal validation data. The DCA curve was further plotted according to the prediction model, with the X-axis showing the predicted threshold probability, the Y-axis showing the net benefit and the red broken line indicating the net benefit of patients at different threshold probabilities. The results showed that the prediction model could obtain net benefit within the threshold range of 0-80%. DCA, decision curve analysis.

or disappeared, the vascular characteristics of the tumor also changed, accompanied by conversion of TIC type. The pCR group showed earlier and more marked downgrading of TIC types than the non-pCR group. After one cycle of NTT, the predominant TIC type in the pCR group changed to the inflow-plateau type (51.6%), and after the final cycle, it further changed to the inflow-inflow type (74.53%). By contrast, in the non-pCR group, the predominant TIC type changed only after the last cycle of NTT, shifting from inflow-outflow at the first two time points to inflow-plateau at the final assessment. Previous studies have similarly shown that, after NAT, TIC patterns in patients with a histologically significant response tend to show downgrading, whereas little or no such change is observed in non-responders (39,40), which is consistent with the present findings.

Malignant tumors generally have high cellular density, which restricts the movement of water molecules within the tissue (41). As NAT progresses, tumor cellularity decreases and water diffusion increases, which can be quantitatively reflected by the ADC value derived from DWI (42). Since ADC values differ significantly between benign and malignant lesions, changes in ADC value may also serve as an indirect indicator of treatment response (13). In the present study, ADC values were higher in the pCR group than those in the non-pCR group at all three MRI time points, and this difference was already evident after the initiation of NTT. In addition, changes in ADC from baseline were greater in the pCR group, and larger ΔADC2 and ΔADC3 values were associated with a higher probability of achieving a pCR after surgery. Previous studies have similarly shown that increases in ADC during NAT have predictive value for pCR (43,44).

However, Park *et al* (13) reported that patients with low ADC values before NAT had a better response to chemotherapy, which differs from the present findings. This discrepancy may be related to the differences in the included study populations. Previous studies of other tumors types have suggested that poor perfusion of antitumor drugs within necrotic tissue may reduce the efficacy of NAT (45). After treatment, reduced

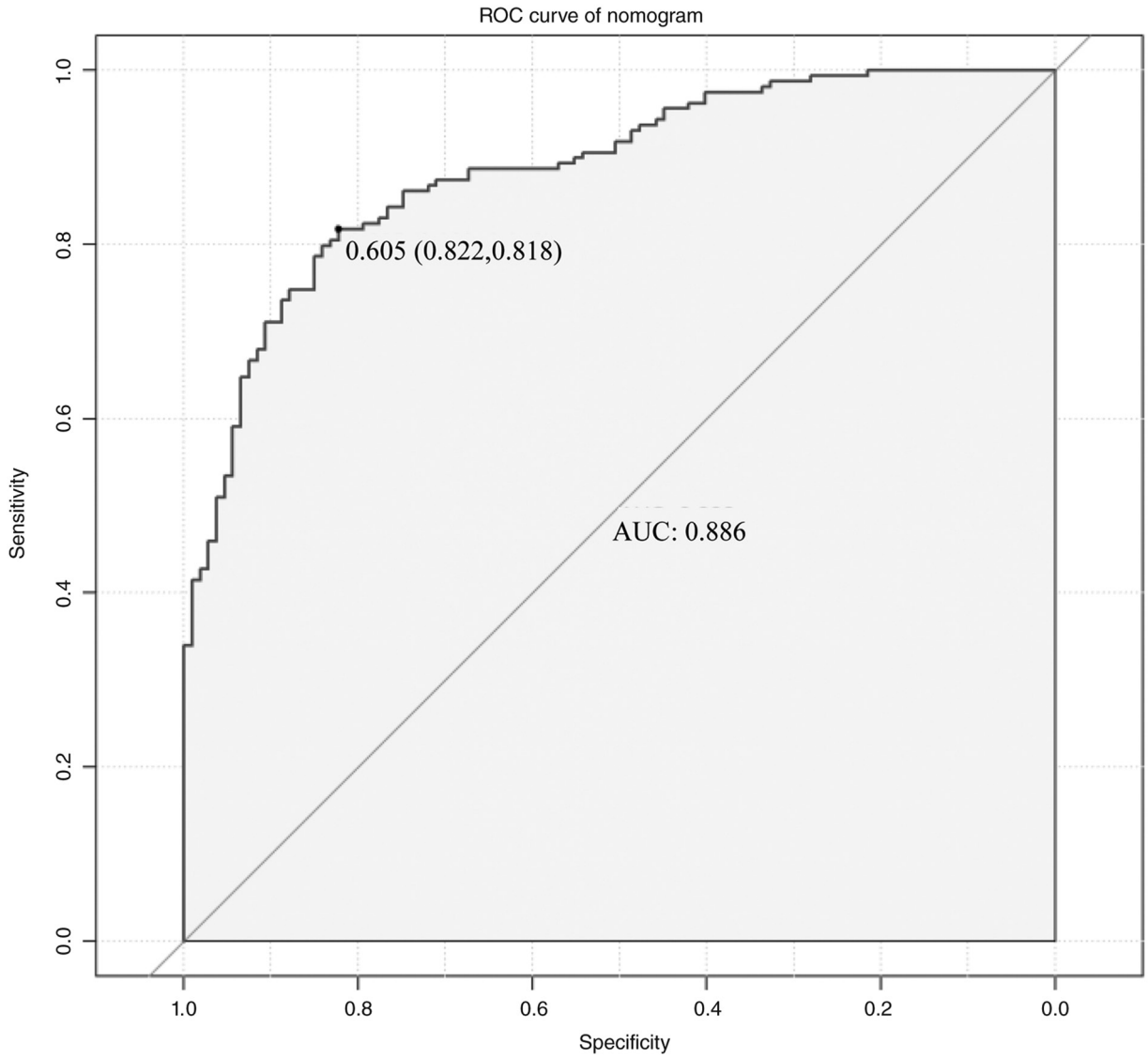

Figure 5. ROC curve of the predictive model from internal validation data. The ROC curve of the pCR prediction model was drawn from internal validation data. The AUC value was 0.886 (P<0.001), the best critical value was 0.605, the sensitivity was 0.822 and the specificity was 0.818, indicating that the prediction ability of the model was good and the accuracy was high. ROC, receiver operating characteristic; AUC, area under the ROC curve.

cellular density in necrotic tissue may lessen restriction of water molecule movement, thereby leading to higher ADC values (12,45). Accordingly, Park *et al* (13) suggested that low ADC values may reflect breast masses with less necrotic tissue and higher cellular density in patients who respond better to NAT. By contrast, it is possible that the tumor cell density in the present cohort was lower than that in the non-pCR group before NAT, resulting in less restricted water diffusion and therefore higher baseline ADC values. However, this possibility was not examined by pathological or cytomolecular analyses in the present study, and further basic investigations are needed to clarify this issue.

In addition to imaging data, hematological markers are often used to evaluate cancer occurrence, progression, treatment efficacy and prognosis (46). However, due to their high sensitivity but limited specificity, single markers are rarely used alone as predictors and are more commonly interpreted in combination with other clinical indicators (28,47,48). In the present study, CEA-0, CEA-1 and CA153-2 were identified as predictive factors for NAT response in HER2-positive BC. CEA is a commonly used broad-spectrum tumor marker in clinical practice (15), whereas CA153 is a traditional marker for BC, with a reported positive rate of 22.5-49.2% in these patients (49). Serum CEA and CA153 levels are higher in malignant than in benign tumors (50), and their concentrations are positively associated with the degree of malignancy (19). Liu *et al* (51) compared CEA and CA153 levels before and after NAT in patients with HER2-positive BC treated with or without trastuzumab. The study found that CEA and CA153 levels were significantly lower in the trastuzumab group than in the non-trastuzumab group, whereas treatment efficacy and prognosis were better in the trastuzumab group (52). Therefore, CEA and CA153 levels may reflect tumor burden in patients with BC, and reductions in tumor burden after treatment may be indirectly reflected by changes in these markers. The present findings were generally consistent with this pattern, as CEA levels in both groups showed a continuous decreasing trend from baseline

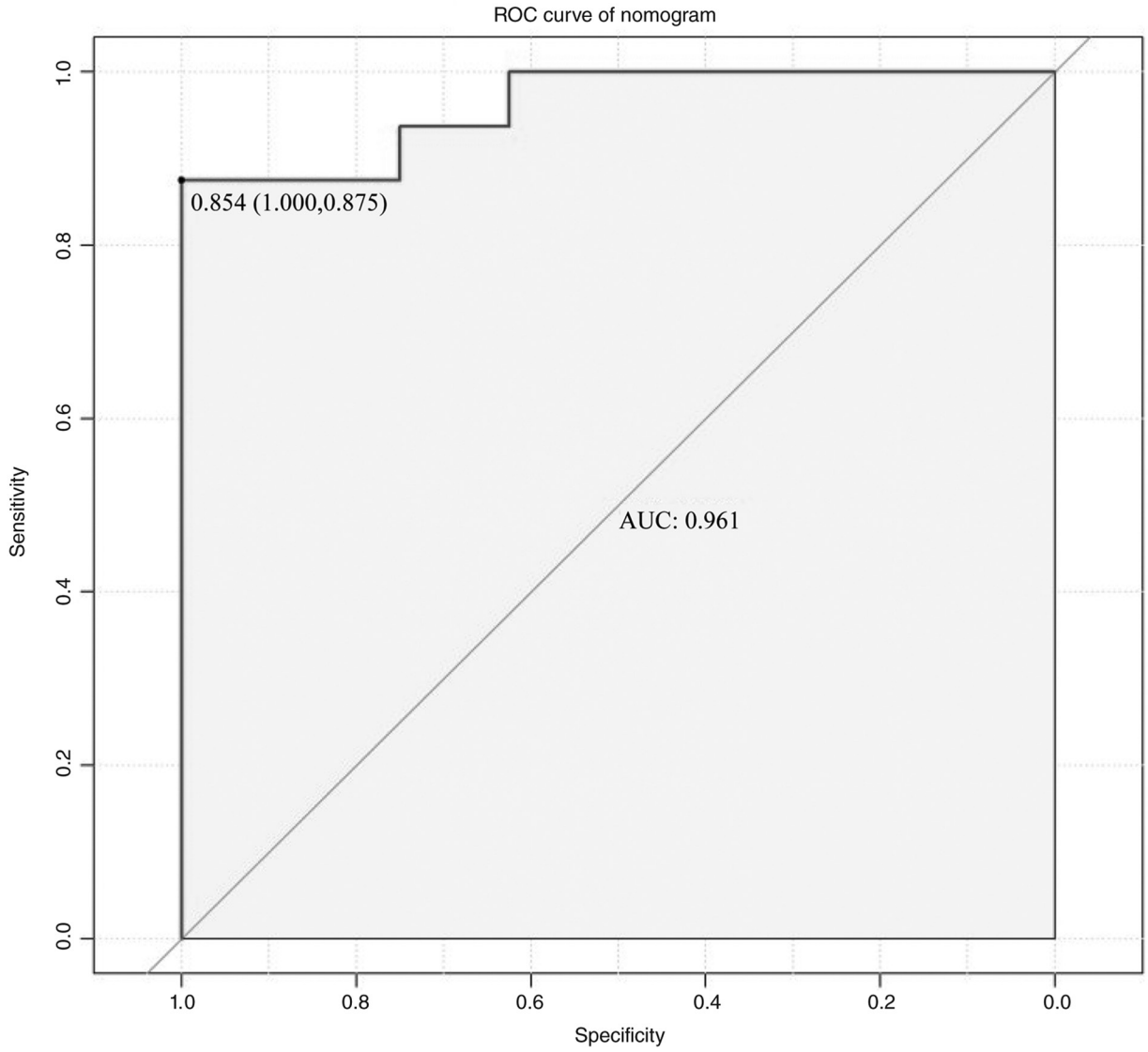

Figure 6. ROC curve of the predictive model from external validation data. A total of 24 patients with human epidermal growth factor receptor 2-positive breast cancer were prospectively collected as the external validation set, and the ROC curve of the external validation set was drawn. The calculated AUC value was 0.961 (P=0.001), the optimum cut-off value was 0.854, the sensitivity was 1.000 and the specificity was 0.875, suggesting that the model's prediction performance was good and accuracy was high in the external validation set. ROC, receiver operating characteristic; AUC, area under the ROC curve.

to after the first targeted therapy and then to the last targeted therapy.

A major strength of the present study is the comprehensive integration of multiple types of clinical data. In addition, rather than relying on cross-sectional data from a single time point, this study was based on dynamic longitudinal observation, allowing more comprehensive use of clinical examination results throughout treatment. The model may help predict whether patients with HER2-positive BC are likely to achieve pCR before surgery during the NAT course. It may also provide a reference for clinicians in treatment planning, including adjustment of NAT duration, selection of surgical timing and approach, and formulation of postoperative adjuvant chemoradiotherapy strategies.

Nevertheless, several limitations should be acknowledged. First, the present study was based on a single-center cohort, and the nomogram was not validated in a larger multicenter external cohort. Second, the largest solid component of the tumor was selected as the study variable, which may not fully represent the entire lesion, as the whole tumor was not measured. Further multi-center studies with larger patient cohorts are needed to validate the predictive performance of this nomogram. In addition, whole-tumor volumetric segmentation or multi-region sampling should be adopted to capture the full heterogeneity of the lesion and to improve the accuracy of pCR prediction based on tumor imaging.

In conclusion, the nomogram developed in the present study, based on PR, ADC2, TIC2, ΔADC2, ΔADC3, CEA-0, CEA-1 and CA153-2, may help predict pCR in patients with HER2-positive BC and may also support individualized treatment decision-making to some extent. By integrating pathological data, imaging parameters and hematological markers obtained during NAT, this combined model may predict postoperative pathological response and provide useful information for prognostic evaluation and subsequent individualized treatment planning in clinical practice. However,

this study has several limitations, including the single-center design and the relatively small sample size. Therefore, further validation in large-scale multicenter cohorts is warranted to optimize the model, and independent cohort studies with rigorous validation are required before clinical application can be considered.

Acknowledgements

Not applicable.

Funding

The present study was financially supported by the First-Class Discipline Team of Kunming Medical University (Kunming Medical University Breast Cancer Precision and Translational Medicine Research Team) (grant no. CXTD202211) and the National Natural Scientific Foundation of China (grant no. 82160532).

Availability of data and materials

The data generated in the present study may be requested from the corresponding author.

Authors' contributions

KZ, ZL, JW and SH conceived and designed the study. KZ, ZL, CW, JW and SZ acquired the data, and KZ, RG and JL performed the statistical analysis and interpreted the data. DC, YT, YD and JN contributed to data interpretation and provided critical intellectual input during manuscript revision. CW, JW and SZ also provided essential study materials and patient data. KZ and SH drafted the manuscript, and all authors (including DC, YT, YD, JN, RG, JL, CW, JW, SZ, ZL and WJ) critically revised it for important intellectual content. WJ, NJ and SH supervised the entire study, obtained funding and were responsible for the overall integrity of the work. KZ, WJ, SH and NJ confirm the authenticity of all the raw data. All authors have read and approved the final manuscript and agree to be accountable for all aspects of the work.

Ethics approval and consent to participate

This study involving human participants was reviewed and approved by the Independent Ethics Committee of Yunnan Cancer Hospital, The Third Affiliated Hospital of Kunming Medical University (Kunming, China; approval no. KYLX2022182). The patients provided written informed consent to participate in this study.

Patient consent for publication

Written informed consent was obtained from the individual(s) for the publication of any potentially identifiable images or data included in this article.

Competing interests

The authors declare that they have no competing interests.

References

1. Bray F, Laversanne M, Sung H, Ferlay J, Siegel RL, Soerjomataram I and Jemal A: Global cancer statistics 2022: GLOBOCAN estimates of incidence and mortality worldwide for 36 cancers in 185 countries. CA Cancer J Clin 74: 229-263, 2024.
2. Harbeck N and Gnant M: Breast cancer. Lancet 389: 1134-1150, 2017.
3. Traub L, Thill M and Nitschmann S: The 20-year results of 5-year hormone therapy in breast cancer: Early Breast Cancer Trialists' Collaborative Group (EBCTCG). Internist (Berl) 56: 410-412, 2018 (In German).
4. Spring LM, Fell G, Arfe A, Sharma C, Greenup R, Reynolds KL, Smith BL, Alexander B, Moy B, Isakoff SJ, *et al*: Complete response after neoadjuvant chemotherapy and impact on breast cancer recurrence and survival: A comprehensive Meta-analysis. Clin Cancer Res 26: 2838-2848, 2020.
5. Haque W, Verma V, Hatch S, Suzanne Klimberg V, Brian Butler E and Teh BS: Response rates and pathologic complete response by breast cancer molecular subtype following neoadjuvant chemotherapy. Breast Cancer Res Treat 170: 559-567, 2018.
6. Blanco SA, Yébenes L, Berjón A and Hardisson D: Evaluation of pathological response to neoadjuvant chemotherapy in breast cancer: Correlation with molecular phenotype. Rev Esp Patol 54: 8-16, 2021 (In Spanish).
7. Harbeck N: Neoadjuvant and adjuvant treatment of patients with HER2-positive early breast cancer. Breast 62 (Suppl 1): S12-S16, 2022.
8. Gianni L, Eiermann W, Semiglazov V, Lluch A, Tjulandin S, Zambetti M, Moliterni A, Vazquez F, Byakhov MJ, Lichinitser M, *et al*: Neoadjuvant and adjuvant trastuzumab in patients with HER2-positive locally advanced breast cancer (NOAH): Follow-up of a randomised controlled superiority trial with a parallel HER2-negative cohort. Lancet Oncol 15: 640-647, 2014.
9. Gianni L, Pienkowski T, Im YH, Tseng LM, Liu MC, Lluch A, Starosławska E, de la Haba-Rodriguez J, Im SA, Pedrini JL, *et al*: 5-year analysis of neoadjuvant pertuzumab and trastuzumab in patients with locally advanced, inflammatory, or early-stage HER2-positive breast cancer (NeoSphere): A multicentre, open-label, phase 2 randomised trial. Lancet Oncol 17: 791-800, 2016.
10. Gianni L, Pienkowski T, Im YH, Roman L, Tseng LM, Liu MC, Lluch A, Staroslawska E, de la Haba-Rodriguez J, Im SA, *et al*: Efficacy and safety of neoadjuvant pertuzumab and trastuzumab in women with locally advanced, inflammatory, or early HER2-positive breast cancer (NeoSphere): A randomised multicentre, open-label, phase 2 trial. Lancet Oncol 13: 25-32, 2012.
11. Baltzer A, Dietzel M, Kaiser CG and Baltzer PA: Combined reading of contrast enhanced and diffusion weighted magnetic resonance imaging by using a simple sum score. Eur Radiol 26: 884-891, 2016.
12. van Ramshorst MS, Loo CE, Groen EJ, Winter-Warnars GH, Wesseling J, van Duijnhoven F, Peeters MTV and Sonke GS: MRI predicts pathologic complete response in HER2-positive breast cancer after neoadjuvant chemotherapy. Breast Cancer Res Treat 164: 99-106, 2017.
13. Park SH, Moon WK, Cho N, Song IC, Chang JM, Park IA, Han W and Noh DY: Diffusion-weighted MR imaging: Pretreatment prediction of response to neoadjuvant chemotherapy in patients with breast cancer. Radiology 257: 56-63, 2010.
14. Kim Y, Kim SH, Song BJ, Kang BJ, Yim KI, Lee A and Nam Y: Early prediction of response to neoadjuvant chemotherapy using dynamic Contrast-enhanced MRI and ultrasound in breast cancer. Korean J Radiol 19: 682-691, 2018.
15. Duffy MJ, Walsh S, McDermott EW and Crown J: Biomarkers in breast cancer: Where are we and where are we going? Adv Clin Chem 71: 1-23, 2015.
16. Nicholson BD, Shinkins B, Pathiraja I, Roberts NW, James TJ, Mallett S, Perera R, Primrose JN and Mant D: Blood CEA levels for detecting recurrent colorectal cancer. Cochrane Database Syst Rev 2015: CD011134, 2015.
17. Grunnet M and Sorensen JB: Carcinoembryonic antigen (CEA) as tumor marker in lung cancer. Lung Cancer 76: 138-143, 2012.
18. Shibata C, Nakano T, Yasumoto A, Mitamura A, Sawada K, Ogawa H, Miura T, Ise I, Takami K, Yamamoto K and Katayose Y: Comparison of CEA and CA19-9 as a predictive factor for recurrence after curative gastrectomy in gastric cancer. BMC Surg 22: 213, 2022.

19. Wang BT and Wang XF: Application value of serum tumor markers combined with dynamic detection in the diagnosis and monitoring of breast cancer. Med Innov China 3: 66-11, 2021 (In Chinese).
20. Dowling GP, Keelan S, Toomey S, Daly GR, Hennessy BT and Hill ADK: Review of the status of neoadjuvant therapy in HER2-positive breast cancer. Front Oncol 13: 1066007, 2023.
21. Amin MB, Edge SB, Greene GL, Byrd DR, Brookland RK, Washington MK, Gershenwald JE, Compton CC, Vega LRM and Gress DM: AJCC cancer staging manual. 8th edition, New York, NY, Springer, 2017.
22. Loibl S and Gianni L: HER2-positive breast cancer. Lancet 389: 2415-2429, 2017.
23. Cortazar P, Zhang L, Untch M, Mehta K, Costantino JP, Wolmark N, Bonnefoi H, Cameron D, Gianni L, Valagussa P, *et al*: Pathological complete response and long-term clinical benefit in breast cancer: The CTNeoBC pooled analysis. Lancet 384: 164-172, 2014.
24. Huang L, Pang D, Yang H, Li W, Wang S, Cui S, Liao N, Wang Y, Wang C, Chang YC, *et al*: Neoadjuvant-adjuvant pertuzumab in HER2-positive early breast cancer: Final analysis of the randomized phase III PEONY trial. Nat Commun 15: 2153, 2024.
25. Kong X, Moran MS, Zhang N, Haffty B and Yang Q: Meta-analysis confirms achieving pathological complete response after neoadjuvant chemotherapy predicts favourable prognosis for breast cancer patients. Eur J Cancer 47: 2084-2090, 2011.
26. Earl H, Provenzano E, Abraham J, Dunn J, Vallier AL, Gounaris I and Hiller L: Neoadjuvant trials in early breast cancer: Pathological response at surgery and correlation to longer term outcomes-what does it all mean? BMC Med 13: 234, 2015.
27. Provenzano E, Bossuyt V, Viale G, Cameron D, Badve S, Denkert C, MacGrogan G, Penault-Llorca F, Boughey J, Curigliano G, *et al*: Standardization of pathologic evaluation and reporting of postneoadjuvant specimens in clinical trials of breast cancer: Recommendations from an international working group. Mod Pathol 28: 1185-201, 2015.
28. Duffy MJ, Harbeck N, Nap M, Molina R, Nicolini A, Senkus E and Cardoso F: Clinical use of biomarkers in breast cancer: Updated guidelines from the European Group on Tumor Markers (EGTM). Eur J Cancer 75: 284-298, 2017.
29. Houssami N, Macaskill P, von Minckwitz G, Marinovich ML and Mamounas E: Meta-analysis of the association of breast cancer subtype and pathologic complete response to neoadjuvant chemotherapy. Eur J Cancer 48: 3342-3354, 2012.
30. Park C, Park K, Kim J, Sin Y, Park I, Cho H, Yang K, Bae BN, Kim KW, Ahn S, *et al*: Prognostic values of negative estrogen or progesterone receptor expression in patients with luminal B HER2-negative breast cancer. World J Surg Oncol 14: 244, 2016.
31. Yang QZ, Lv YL, Mu WM and Li Y: Effect of hormone receptor status on Her-2 positive breast cancer. Chin J Med Sci 4: 15-19, 2022 (In Chinese).
32. Li JL and Zhu DM: The Value of TAP Content in Peripheral Blood in Predicting the Efficacy of Neoadjuvant Chemotherapy for Her-2 Positive Breast Cancer. J Jinzhou Med Univ 6: 51-55, 2022 (In Chinese).
33. McDermott MSJ, Canonici A, Ivers L, Browne BC, Madden SF, O'Brien NA, Crown J and O'Donovan N: Dual inhibition of IGF1R and ER enhances response to trastuzumab in HER2 positive breast cancer cells. Int J Oncol 50: 2221-2228, 2017.
34. Luo Y and Huang J: New Mechanism of ER-α36 Mediating Trastuzumab Resistance in Breast Cancer. Med Recapitulate 27: 1722-1727, 2021 (In Chinese).
35. Bitencourt AGV, Gibbs P, Rossi Saccarelli C, Daimiel I, Lo Gullo R, Fox MJ, Thakur S, Pinker K, Morris EA, Morrow M and Jochelson MS: MRI-based machine learning radiomics can predict HER2 expression level and pathologic response after neoadjuvant therapy in HER2 overexpressing breast cancer. EBioMedicine 61: 103042, 2020.
36. Mermut O, Inanc B, Gursu RU, Arslan E, Trabulus DC, Havare SB and Ulusan MB: Factors affecting pathological complete response after neoadjuvant chemotherapy in breast cancer: A single-center experience. Rev Assoc Med Bras (1992) 67: 845-850, 2021.
37. Wahl RL, Jacene H, Kasamon Y and Lodge MA: From RECIST to PERCIST: Evolving Considerations for PET response criteria in solid tumors. J Nucl Med 50 (Suppl 1): 122S-150S, 2009.
38. Kuhl CK, Mielcareck P, Klaschik S, Leutner C, Wardelmann E, Gieseke J and Schild HH: Dynamic breast MR imaging: Are signal intensity time course data useful for differential diagnosis of enhancing lesions? Radiology 211: 101-110, 1999.
39. Xu HD and Zhang YQ: Evaluation of the efficacy of neoadjuvant chemotherapy for breast cancer using diffusion-weighted imaging and dynamic contrast-enhanced magnetic resonance imaging. Neoplasma 64: 430-436, 2017.
40. Nie Y, He Y, Wang J, Zhang H and Su J: MRI Images-Based evaluation of efficacy of neoadjuvant chemotherapy for breast cancer and its effect on depression and immune function of patients. Contrast Media Mol Imaging 2022: 8685680, 2022.
41. Iima M, Honda M, Sigmund EE, Ohno Kishimoto A, Kataoka M and Togashi K: Diffusion MRI of the breast: Current status and future directions. J Magn Reson Imaging 52: 70-90, 2020.
42. Gao W, Guo N and Dong T: Diffusion-weighted imaging in monitoring the pathological response to neoadjuvant chemotherapy in patients with breast cancer: A meta-analysis. World J Surg Oncol 16: 145, 2018.
43. Li XR, Cheng LQ, Liu M, Zhang YJ, Wang JD, Zhang AL, Song X, Li J, Zheng YQ and Liu L: DW-MRI ADC values can predict treatment response in patients with locally advanced breast cancer undergoing neoadjuvant chemotherapy. Med Oncol 29: 425-431, 2012.
44. Hottat NA, Badr DA, Lecomte S, Besse-Hammer T, Jani JC and Cannie MM: Value of diffusion-weighted MRI in predicting early response to neoadjuvant chemotherapy of breast cancer: Comparison between ROI-ADC and whole-lesion-ADC measurements. Eur Radiol 32: 4067-4078, 2022.
45. Humphries PD, Sebire NJ, Siegel MJ and Olsen ØE: Tumors in pediatric patients at diffusion-weighted MR imaging: Apparent diffusion coefficient and tumor cellularity. Radiology 245: 848-854, 2007.
46. Yilihamu Y, Wang L, Ma T, Zhao T, Wang Y and Sun G: The effects of preoperative serum carcinoembryonic antigen, cancer antigen 15-3 and cancer antigen 125 on the prognosis of breast cancer patients with different molecular subtypes. J Clin Med Res 16: 491-502, 2024.
47. Crosby D, Bhatia S, Brindle KM, Coussens LM, Dive C, Emberton M, Esener S, Fitzgerald RC, Gambhir SS, Kuhn P, *et al*: Early detection of cancer. Science 375: eaay9040, 2022.
48. Chen S, Zeng J, Gong K, Liu Y, Long S, Han L and Luo D: A novel four-serum marker model for early detection and therapeutic monitoring of breast cancer. Sci Rep 16: 614, 2025.
49. Xu SX, Huo QY, Zhang MY, Wei YH, Yang Y Ji JH, Zhang CF and Zhao BY: Clinical value of combined serum CAl53, CEA, SF, CT and Hcy in the diagnosis of breast cancer. J Mol Diagn Ther 12: 190-194, 2020 (In Chinese).
50. Wu B, Zhu H, Sha DH and Guo YT: Study on diagnostic value of DWI combined with serum carbohydrate antigen 153, 125 and carcinoembryonic antigen in breast cancer. J Med Imaging 31: 1326-1329, 1346, 2021 (In Chinese).
51. Liu RJ: The Effect of Trastuzumab in the Treatment of HER-2 Positive Advanced Breast Cancer and its Effect on Serum CEA and CA153 Levels. J Med Inform 34: 125-127, 2021 (In Chinese).
52. Tarighati E, Keivan H and Mahani H: A review of prognostic and predictive biomarkers in breast cancer. Clin Exp Med 23: 1-16, 2023.